Comparison of high cloud characteristics as estimated by selected spaceborne observations and ground-based lidar datasets

Artemio Plana-Fattori, Gérard Brogniez, Patrick Chervet, Martial Haeffelin, Olga Lado-Bordowsky, Yohann Morille, Frédéric Parol, Jacques Pelon, Antoine Roblin, Geneviève Sèze, et al.

Comparison of High-Cloud Characteristics as Estimated by Selected Spaceborne Observations and Ground-Based Lidar Datasets

ARTEMIO PLANA-FATTORI,[*,+] GÉRARD BROGNIEZ,[#] PATRICK CHERVET,[@] MARTIAL HAEFFELIN,[&,**] OLGA LADO-BORDOWSKY,[++] YOHANN MORILLE,[**,##] FRÉDÉRIC PAROL,[#] JACQUES PELON,[*,@@] ANTOINE ROBLIN,[@] GENEVIÈVE SÈZE,[##,@@] AND CLAUDIA STUBENRAUCH[**,##]

[*] *Centre National de la Recherche Scientifique, Laboratoire Atmosphères, Milieux, Observation Spatiale, Vélizy-Villacoublay, France*
[+] *Université de Versailles Saint-Quentin-en-Yvelines, Vélizy-Villacoublay, France*
[#] *Laboratoire d'Optique Atmosphérique, CNRS, Villeneuve d'Ascq, France*
[@] *Département d'Optique Théorique et Appliquée, ONERA, Palaiseau, France*
[&] *CNRS, Institut Pierre Simon Laplace, Palaiseau, France*
[**] *Ecole Polytechnique, Palaiseau, France*
[++] *Ecole Nationale Supérieure des Sciences Appliquées et de Technologie, Lannion, France*
[##] *Laboratoire de Météorologie Dynamique, CNRS, Palaiseau and Paris, France*
[@@] *Université Pierre et Marie Curie, Paris, France*

(Manuscript received 15 February 2008, in final form 7 January 2009)

ABSTRACT

The characterization of high clouds as performed from selected spaceborne observations is assessed in this article by employing a number of worldwide ground-based lidar multiyear datasets as reference. Among the latter, the ground lidar observations conducted at Lannion, Bretagne (48.7°N, 3.5°W), and Palaiseau, near Paris [the Site Instrumental de Recherche par Télédétection Atmosphérique (SIRTA) observatory: 48.7°N, 2.2°E], both in France, are discussed in detail. High-cloud altitude statistics at these two sites were found to be similar. Optical thicknesses disagree, and possible reasons were analyzed. Despite the variety of instruments, observation strategies, and methods of analysis employed by different lidar groups, high-cloud optical thicknesses from the Geoscience Laser Altimeter System (GLAS) on board the *Ice, Cloud and land Elevation Satellite* (*ICESat*) were found to be consistent on the latitude band 40°–60°N. Respective high-cloud altitudes agree within 1 km with respect to those from ground lidars at Lannion and Palaiseau; such a finding remains to be verified under other synoptic regimes. Mean altitudes of high clouds from Lannion and Palaiseau ground lidars were compared with altitudes of thin cirrus from the Television and Infrared Observation Satellite (TIROS) Operational Vertical Sounder (TOVS) Path-B 8-yr climatology for a common range of optical thicknesses (0.1–1.4). Over both sites, the annual altitude distribution of thin high clouds from TOVS Path-B is asymmetric, with a peak around 8–9.5 km, whereas the distribution of high clouds retrieved from ground lidars seems symmetric with a peak around 9.5–11.5 km. Additional efforts in standardizing ground lidar observation and processing methods, and in merging high-cloud statistics from complementary measuring platforms, are recommended.

1. Introduction

The observation of geophysical variables requires temporal and spatial resolutions that can resolve the main features of the object under consideration. On one hand, Earth would appear bluish for human observers on the orbits of Mars and Jupiter, and such an appearance would be the same after minutes or after days of observation. On the other hand, the in situ observation of cloud particles needs high time resolution because cloud layers are not homogeneous and research aircraft travel at many meters per second. Intermediate scales to these two examples are considered in this article, in terms of the characterization of high-altitude clouds (hereinafter high clouds) from ground-based and spaceborne instruments.

High clouds are crucially important to global radiative processes and to the thermal balance of the earth. While thick high clouds, with a global coverage of only about 5% (Rossow and Schiffer 1999; Stubenrauch et al. 2006),

Corresponding author address: Artemio Plana-Fattori, Laboratoire Atmosphères, Milieux, Observation Spatiale, 10–12 Ave. de l'Europe, 78140 Vélizy-Villacoublay, France.
E-mail: artemio.planafattori@latmos.ipsl.fr

DOI: 10.1175/2009JAMC1964.1

are important for the water cycle, optically thin cirrus clouds, because of their large spatial coverage (Wylie and Menzel 1999; Stubenrauch et al. 2006), have an impact on the radiative budget (McFarquhar et al. 2000), and they play an important role in the dehydration of air entering the stratosphere (Dessler and Yang 2003).

Now that more and more instruments in orbit are providing years of cloudiness data [e.g., the Cloud-Aerosol Lidar with Orthogonal Polarization (CALIOP) on board the A-Train satellite constellation; Winker et al. (2007)], a challenging task is evaluating such globally consistent information. A first motivation for this study is hence to learn more about the differences existing between high-cloud statistics resulting from a variety of measuring systems. More specifically, we compare high-cloud altitudes from one lidar in space [the Geoscience Laser Altimeter System (GLAS) on board the *Ice, Cloud and land Elevation Satellite* (*ICESat*)], from a series of Television and Infrared Observation Satellite (TIROS-N) Operational Vertical Sounder (TOVS) spaceborne instruments, and from a couple of ground lidars in France. Also, high-cloud optical thicknesses from GLAS are compared similarly from a number of worldwide multiyear ground-based lidar datasets.

The second motivation comes from the fact that high clouds strongly affect the performances of any airborne electro-optical sensor for limb-viewing observations. Chervet and Roblin (2006) have developed a model to determine the performance limitations of an electro-optical system due to the statistical presence of high clouds along the line of sight. The model has been applied to various locations and seasons, using the cloud climatology of the TOVS Path-B dataset (Stubenrauch et al. 2006). Airborne sensor performances can be significantly impacted by very thin ice clouds (visible optical depth <0.1) especially for lines of sight close to the horizon, but such clouds cannot be determined by IR sounders on board satellites using nadir-viewing geometries (Wylie et al. 1994; Stubenrauch et al. 2005). Ground lidars are well adapted to detect clouds associated with small optical thicknesses; hence, they can be used to improve the climatologic data gathered by radiometers on board satellites (Platt et al. 1994). Nevertheless, their measurements are restricted to a few locations and their detection performances at high altitude are limited by lower-atmospheric layers (aerosol, cloud) and by ambient light. Spaceborne lidars are well suited for observing high thin clouds: their signal is not attenuated by lower layers, and their observations are not limited to a few locations (Winker and Trepte 1998). However, when they are operated from space, lidar systems are limited by atmospheric backscattered signals that have low signal-to-noise ratios on optically thin targets (Chazette et al. 2001). Improvement in our understanding of high-cloud statistics can be reached by coupling ground-based and spaceborne observations as well as different types of instruments.

Our main goal is to intercompare the distributions of the optical thickness and altitude of high clouds as seen by selected spaceborne observations to those obtained from ground lidar datasets. Because of the variety of instrumentation, strategies, and methods applied to lidar measurements, we first devoted a significant effort toward comparing ground lidar datasets. The article is organized as follows. Datasets under consideration are summarized in section 2. A number of comparisons involving high-cloud optical thicknesses and altitudes are presented in sections 3 and 4, respectively. Our main findings are summarized in section 5, together with recommendations for future work.

2. Datasets

a. Ground-based lidar at Palaiseau and Lannion

Lidar observations have been conducted at Palaiseau (48.7°N, 2.2°E) as automatically as possible, under all rainless atmospheric conditions. The Site Instrumental de Recherche par Télédétection Atmosphérique (SIRTA) observatory deploys a dual-wavelength polarization lidar named the Lidar Nuages Aerosols (LNA, for cloud and aerosol lidar). The LNA's vertical resolution is 15 m and the detected wavelengths are 532 nm (parallel and cross polarized) and 1064 nm (Haeffelin et al. 2005). The LNA backscattered signal provides information on the presence of clouds and aerosols in the vertical column between instrument level and 15-km altitude. An algorithm based on wavelet transform analysis (Morille et al. 2007) is applied to analyze all lidar profiles and retrieve the vertical structures of clouds and aerosols layers. Two independent methods described by Cadet et al. (2005) are applied to estimate the optical thickness of each cloud layer: molecular integration (MI) and particle integration (PI). The former integrates the difference (interpreted as extinction) between the experimental backscatter signal and the theoretical molecular lidar return, while the latter integrates the experimental backscatter signal after assuming a ratio (the lidar ratio) between the extinction and backscattering coefficients. The MI method does not require any hypotheses about cloud layer microphysics but strongly depends on the accuracy of the estimated molecular lidar return throughout the cloud layer. This method has been discussed in detail by Young (1995). On the other hand, the PI method is less sensitive to the signal-to-noise ratio and does not need to be normalized in particle-free layers but does require the

specification of the lidar ratio, which is assumed to be temperature dependent. We have adopted the relationship applied by Noel et al. (2007), and it provides values of about 18.9, 21.4, and 22.7 sr at temperatures of −20°, −40°, and −60°C, respectively. A similar approach using MI and PI methods is followed in analyzing the GLAS observations (Palm et al. 2002).

Lidar observations have been conducted at Lannion (48.7°N, 3.5°W) through short and numerous campaigns, mainly driven by National Oceanic and Atmospheric Administration (NOAA) Advanced Very High Resolution Radiometer (AVHRR) overpasses and the lack of low-level clouds. Observations are performed with a 532-nm backscattering and depolarization lidar system above the Ecole Nationale Supérieure des Sciences Appliquées et de Technologie (ENSSAT) building. The vertical resolution is 30 m. Optical thicknesses associated with cloud layers were estimated by applying an MI method similar to that employed at SIRTA.

Briefly, ground-based lidar observations have been conducted at Lannion and Palaiseau for use in a variety of atmospheric studies, following different strategies and methods. With the aim of comparing high-cloud characteristics from other observation systems (ground based and space borne), these two datasets were compiled to be as similar as possible. Both datasets became available for this study in the form of time–altitude distributions, describing thousands of cloud layers identified over more than 3 yr at each site. For each atmospheric profile, the top and base altitudes were taken as those from the highest and the lowest cloud layers, respectively. Mean altitudes were computed as the arithmetic average of the respective top and base altitudes, and the geometrical thickness as their difference. Atmospheric conditions associated with cloud-base altitudes below 7 km were discarded. The high-cloud optical thickness was computed for the remaining conditions, by summing the respective layer contributions provided by the MI–PI methods. Only optical thicknesses ranging from 0.003 up to 3 were retained, that is, up to a typical optical thickness for lidar attenuation-limited opaque cirrostratus (Sassen and Cho 1992). Remaining observations were grouped by day, and all the days corresponding to less than 10 observations associated with high clouds were discarded. This rejection filter was applied to avoid undersampled, or too transient, meteorological conditions; in the case of Palaiseau (integration time of 30 s), such a number of observations corresponds to at least 5 min of high-cloud cover (continuous or not).

Retained optical thicknesses were then corrected as suggested by Chen et al. (2002) to include a first-order approximation of the multiple scattering effects on backscatter profiles. Such a correction accounts for the very intense forward scattering (toward the lidar receiver) of photons that have been previously backscattered after a first interaction. According to this method, experimentally derived optical thicknesses TAU are hereinafter interpreted as their corrected value, exp(TAU) − 1. The importance of such a correction is strongly dependent on the magnitude of TAU; for example, experimental values equal to 0.01, 0.1, and 1 become 0.0101, 0.105, and 1.72, respectively.

The remaining days are hereinafter analyzed as independent samples of high-cloud cover (base altitude above 7 km) with no cloud layer underneath. The restriction of our interest to the daily characteristics of high-cloud cover (rather than on the overall ensemble of lidar-derived data) effectively reduced the sample sizes under consideration: 69 (193) days corresponding to at least 10 observations associated with high clouds at Lannion (Palaiseau) rather than the 18 021 (31 445) atmospheric profiles associated with them. Such a statistical treatment can be justified by the fact that these datasets correspond to different time resolutions (30 s for Palaiseau, and from 2 to 32 s depending on the date for Lannion). A suite of parameters was obtained from the 10 (or frequently much more) observations associated with high clouds on each day: the number of observations under consideration, the daily limits of the high-cloud cover (lowest base and highest top altitudes), and finally the daily minimum, mean, maximum, and standard deviation values of the mean altitude, the geometrical thickness, and the optical thickness of high clouds.

Table 1 summarizes the observations with high clouds under consideration throughout this study. Seasonal sampling was less uniform at Lannion, and the overall number of days with available observations was smaller than at Palaiseau. At the former site the lidar operations were basically conducted during short campaigns, while the latter site is a routine observation facility (Haeffelin et al. 2005). Coherently, 90% (36%) of the available days correspond to at least 10 observations associated with high clouds in the case of Lannion (Palaiseau). A subset of dataset A is compared with other ground lidar sites and GLAS results, as is subdataset B with TOVS Path-B altitude estimates. Except for the ground lidar results from Gadanki, India; Haute Provence, France; Réunion island in the Indian Ocean; and the Southern Great Plains Cloud and Radiation Testbed in the Midwestern United States (SGP CART) (see Table 3), all the comparisons account for cloud optical thickness values that were previously corrected by multiple-scattering effects. High clouds under consideration in subdataset B match as closely as possible the optically thin ice clouds

TABLE 1. Summary of Lannion and Palaiseau datasets of ground lidar observations. DJF stands for December–January–February, and so on. Full datasets correspond to all the available observations at the beginning of this study. Subdataset A (B) corresponds to clouds whose base altitude was higher than 7 (8) km and whose experimental optical thickness, i.e., before any multiple scattering correction, was between 0.003 and 3 (0.095 and 0.88). Respective numbers of days corresponding to at least 10 observations and the numbers of observations under consideration in each case are also indicated.

	Lannion (Sep 2001–Jun 2005)					Palaiseau (Oct 2002–Feb 2006)				
	DJF	MAM	JJA	SON	Total	DJF	MAM	JJA	SON	Total
Full dataset (days)	8	13	36	20	77	126	136	111	161	534
Subdataset A (days)	8	12	30	19	69	24	48	58	63	193
Relative to full dataset (%)	100	92	83	95	90	19	35	52	39	36
No. of observations	1763	1561	7536	7161	18 021	5035	10 820	6572	9018	31 445
Subdataset B (days)					37					79
Relative to full dataset (%)					48					15
Relative to subdataset A (%)					54					39
No. of observations					6621					7396

that are retrieved by the TOVS Path-B algorithm: base above 8 km and corrected optical thickness between 0.1 and 1.4 (see section 2d).

Figure 1 presents the subset of dataset A's observations associated with high clouds at Lannion and Palaiseau. On a given day, the number of observations associated with high clouds can be smaller than 10: high-cloud cover was absent or negligible during lidar operation, or simply the lidar system was not operating. The daily variability of the number of observations with high clouds is significant given that high-cloud cover is naturally variable, and lidar operation can be interrupted. On average, high-cloud base altitudes are slightly lower and the top altitudes slightly higher at Lannion than at Palaiseau, with median values of about 7.02 and 7.55 km and of 12.00 and 11.46 km, respectively. Such a result has no apparent reason, although sampling strategy cannot be excluded. The three bottom panels compare the optical thicknesses estimated after applying the MI method to both datasets (Lannion versus Palaiseau, MI method), as well as the optical thicknesses estimated after applying two approaches to the same dataset (Palaiseau, MI and PI methods).

The MI method provided a larger range of values at Lannion (0.01–2.03) than at Palaiseau (0.02–0.70) and similar median values (about 0.14); it is challenging to evaluate the importance of instrumentation issues and algorithm particularities. At Palaiseau, optical thicknesses from the MI method are on average higher than those from the PI method, with median values about 0.14 and 0.09, respectively. As shown in Fig. 2, optical thicknesses from these two methods can be very different for a given day. Their correlation coefficient is weak (about 0.35). Figure 2 shows also that the daily variability of the optical thicknesses is very high (standard deviation values are displayed as gray error bars). Such variability can result from a combination of factors, including instrument uncertainties and the nonsteady nature of the high-cloud cover above the site.

b. Ground-based lidar at selected sites

High clouds have been observed worldwide with the help of surface-based lidar instrumentation. Many observation initiatives have been put into place for periods covering a few hours up to a couple of years, for a variety of regional–seasonal motives and goals. A nonexhaustive selection is presented in Table 2. Unfortunately, the time coverage of most of these initiatives was shorter than 1 yr, reducing their meaningfulness for climatologic purposes.

A second class of studies has been based on the atmospheric monitoring over years at permanent sites. The advantages of this strategy are somewhat obvious: uniform sampling of weather systems and of seasonal features become possible, while the statistical robustness of the datasets created is increased. Long-term funding is involved and high scientific standards are required. As a consequence, only a few such datasets have been established. Sassen et al. (2001) have summarized the longest of them, namely that of the University of Utah's Facility for Atmospheric Remote Sensing (FARS) near Salt Lake City. Many years of observation have been successfully analyzed to fully characterize high clouds (Sassen and Benson 2001; Sassen and Campbell 2001; Sassen and Comstock 2001; Sassen et al. 2003, 2007).

A summary of the datasets under consideration is provided in Table 3. Only datasets spread over at least 2 yr and sampling all the seasons were taken into account. Table 3 gives an overview of seven ground-based lidar observation datasets: two tropical sites in the Indian Ocean region (Gadanki, India, and Réunion Island) and five midlatitude sites, two of them in continental United States (Salt Lake City, and the Atmospheric Radiation

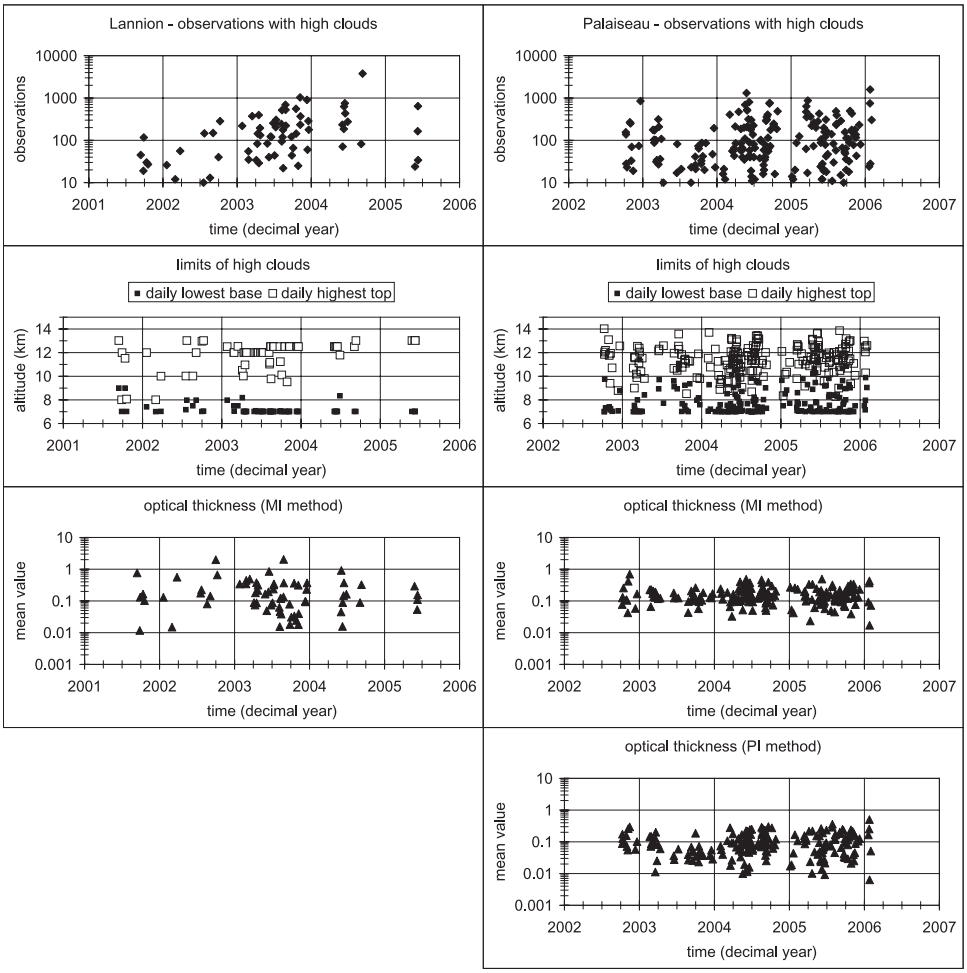

FIG. 1. Distribution of high clouds under consideration (left) Lannion (observations between September 2001 and June 2005) and (right) Palaiseau (observations between October 2002 and February 2006): (top to bottom) daily number of observations with high clouds, daily limits of high clouds, and daily mean values of their optical thicknesses. The MI method for obtaining optical thicknesses was considered in both cases, and the PI method was used in the case of Palaiseau only.

Measurement Program's SGP CART site in Oklahoma), and three in France (Haute Provence, Lannion, and Palaiseau). These sites correspond to different landscapes, including rural (Gadanki, Haute Provence, SGP CART), urban (Lannion, Réunion, Salt Lake City), and a somewhat intermediate situation (Palaiseau); moreover, one of them can be classified as oceanic (Réunion), another is located a few kilometers from the sea (Lannion), and two others are located near mountain features (Haute Provence, Salt Lake City). Each dataset resulted from the application of a particular observation strategy, from automatic recording to human-dependent visual identification of ice clouds prior to lidar operation. Moreover, a particular data-processing chain was applied to each dataset, providing results to the community in a variety of formats.

c. *Spaceborne lidar*

Global spaceborne lidar profiling of atmospheric clouds and aerosol began in 2003 with the launch of the GLAS on board *ICESat* (Spinhirne et al. 2005a). GLAS was the first spaceborne lidar system for which the optical thickness of semitransparent clouds was operationally produced. The characteristics of high clouds from GLAS observations have been presented by Eguchi et al. (2007); for instance, their optical thickness is typically greater in the midlatitudes. In the present study, only the second long period of GLAS observations (between 1 October and 18 November 2003) is taken under consideration. As in Eguchi et al. (2007), we have analyzed the ''laser 2a campaign,'' ignoring its first 7 days, for which the data quality was poor. During

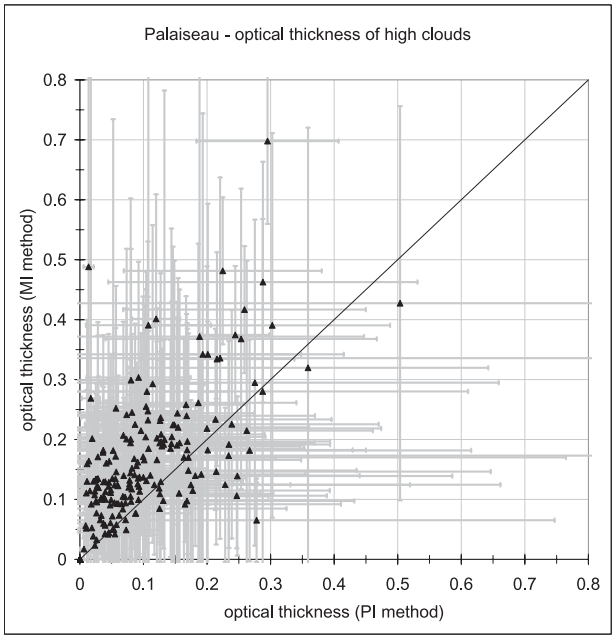

FIG. 2. Scatterplot of high-cloud optical thicknesses at Palaiseau obtained simultaneously after application of the PI (abscissas) and MI (ordinates) methods. Black triangles and gray bars indicate daily mean and standard deviation values, respectively. The one-to-one correspondence line is also displayed.

this period the 532-nm channel was at its uppermost sensitivity (Abshire et al. 2005; Schutz et al. 2005). GLAS measurements are performed with a 65-m-diameter footprint and 172-m along-track spacing (Schutz et al. 2005). We use GLAS Release-26 products, obtained from the 1-s-averaged data (40 single profiles). Each averaged profile corresponds to a 7-km along-track narrow segment.

Methods employed in analyzing GLAS observations are described by Palm et al. (2002), and they are similar to the methods used for the ground-based retrievals. The processing algorithms employ two independent procedures to derive the cloud optical thickness depending on atmospheric conditions. For optically thin layers (TAU $<$ 0.6), or for cases where the lower boundary of the layer is close to the surface or within 1 km of another aerosol or cloud layer, a forward-integration solution of the lidar equation (as in the PI method) is employed using the cloud extinction-to-backscatter ratio (lidar ratio) obtained from lookup tables. For sufficiently isolated cloud layers within an approximate TAU range of 0.1–2, the lidar ratio and TAU can be independently derived from the loss of signal relative to the known molecular scattering value just below the cloud (Hlavka et al. 2005) as in the MI method. Multiple scattering has been considered by assuming a correction factor depending on the optical thickness, particle size, geometric depth, and mean height of the layer (Palm et al. 2002). As a result, cloud optical thicknesses can be determined down to about 0.002 at night, whereas this limit is about 0.02 for daytime observations (Hlavka et al. 2005, and our Fig. 5).

d. Spaceborne infrared vertical sounder

The TOVS Path-B dataset (Scott et al. 1999; Stubenrauch et al. 2006) provides global atmospheric temperature and water vapor profiles as well as cloud and surface properties at a spatial resolution of 1° latitude $\times$ 1° longitude. At present, the dataset covers the time period from 1987 to 1995. Cloud pressure P_{cld} and effective IR cloud emissivity E_{cld} are retrieved by applying a weighted chi-2 method to five radiances along the 15-μm CO_2 absorption band (Stubenrauch et al. 1999a). The relatively high spectral resolution of the TOVS instruments yields reliable cirrus properties, day and night (Stubenrauch et al. 1999b, 2006). The High Resolution Infrared Radiation Sounder (HIRS) component of the TOVS package is sensitive to clouds associated with visible optical thicknesses above 0.1 (Wylie and Menzel 1999). Cloud altitude has been evaluated (Stubenrauch et al. 2005) with vertical profiles of backscattered radiation from quasi-simultaneous Lidar In-Space Technology Experiment (LITE) observations (McCormick et al. 1993). The cloud altitude determined by TOVS generally corresponds well to the ''apparent middle altitude'' of the cloud system at 1° (latitude and longitude) spatial resolution. According to TOVS Path-B, about 30% of the globe is covered by high clouds (defined as $P_{\text{cld}} < 440$ hPa), and 28% of the Northern Hemisphere (NH) midlatitudes are covered by high clouds. The seasonal cycle of high-cloud amount in the NH midlatitudes is stronger over land than over ocean. There are more high clouds in spring and in summer (up to 35%) than in autumn and in winter (less than 25%).

In the following, only optically thin cirrus ($E_{\text{cld}} < 0.5$, corresponding approximately to visible optical thickness $<$1.4) is compared to high-cloud statistics from lidar measurements. About 40% of all high clouds included in the TOVS Path-B statistics fall into this category. High clouds in this analysis are defined as clouds at altitudes above 8 km (corresponding approximately to 380 hPa). For the comparison with lidar measurements, P_{cld} had to be transformed into altitude by using the TOVS Path-B monthly mean profiles of virtual temperature. The altitude determination of thin cirrus is more uncertain than for thicker cirrus. Stubenrauch et al. (2008) have applied the weighted chi-2 method to data from the Atmospheric IR Sounder (AIRS) on board the *Aqua* satellite (Chahine et al. 2006) and compared the retrieved cloud height with collocated

TABLE 2. Selected high-cloud observations from surface-based lidar instrumentation.

Source	Location	Period	Remarks
Ansmann et al. (1993)	North Sea (53.5°–55°N, 7°–9°E)	Sep–Oct 1989	Four lidar systems; 38 cirrus cases
Beyerle et al. (1998)	Atlantic Ocean (45°S–35°N, 25°–30°W)	Oct–Nov 1996	57 h in the tropics (72% with cirrus)
Beyerle et al. (2001)	Table Mountain, CA(34.4°N, 117.7°W)	Feb–Mar 1997	Three lidar systems; ~200 h with cirrus
Chen et al. (2002)	Chung-Li, Taiwan (25°N, 121°E)	Aug 1999–Jul 2000	210 mean profiles with cirrus
Comstock et al. (2002)	Republic of Nauru (0.5°S, 166.9°E)	Apr–Nov 1999	5664 h (44% with high clouds)
Del Guasta et al. (1993)	Dumond d'Urville, Antarctica (66°S, 140°E)	1989–90 (1 yr)	2770 mean profiles with cirrus
Flamant et al. (1989)	Haute Provence, France (43.9°N, 5.7°E)	1983–84	A few weeks of observation
Giannakaki et al. (2004)	Thessaloniki, Greece (40.5°N, 22.9°E)	Sep 2001–Oct 2002	Seven cirrus cases
Gobbi et al. (2004)	Rome, Italy (41.8°N, 12.6°E)	Feb 2001–Feb 2002	993 mean profiles (45% with cirrus)
Imasu and Iwasaka (1991)	Nagoya, Japan (35.2°N, 137.0°E)	1987–88	Two periods of intensive observation
Immler and Schrems (2002b)	Punta Arenas, Chile (53.1°S, 70.9°W)	Mar–Apr 2000	71 h (56% with cirrus)
Immler and Schrems (2002b)	Prestwick, Scotland (55.5°N, 4.6°W)	Sep–Oct 2000	74 h (35% with cirrus)
Immler and Schrems (2002a)	Atlantic Ocean (8°S–12°N)	30 May–3 Jun 2000	"One single cloud across 2200 km"
Pace et al. (2003)	Mahe, Seychelles (4.4°S, 55.3°E)	Feb–Mar 1999	67 h with cirrus
Parameswaran et al. (2004)	Gadanki, India (13.5°N, 79.2°E)	Jan 1999–Mar 2000	121 nights with cirrus
Platt (1973)	Adelaide, Australia (34.9°S, 138.6°E)	Nov 1970	Four cirrus cases
Platt and Dilley (1979)	Adelaide, Australia (34.9°S, 138.6°E)	May 1972	Three cirrus cases
Platt and Dilley (1979)	Aspendale, Australia (38°S, 144°E)	Sep–Nov 1975	Five cirrus cases
Platt et al. (1987)	Aspendale, Australia (38°S, 144°E)	1978–80	22 winter and 26 summer cirrus cases
Platt et al. (1987)	Darwin, Australia (12.4°S, 130.8°E)	Mar–Apr 1981	11 cirrus cases
Platt et al. (1994)	Global (ECLIPS project)	1989, 1991	Two periods of intensive observation
Platt et al. (1998)	Kavieng, Papua New Guinea (2.5°S, 152°E)	Jan–Feb 1993	14 cirrus cases
Platt et al. (2002)	Melville Island, Australia (11.4°S, 130.4°E)	Nov–Dec 1995	19 cirrus cases
Reichardt (1999)	Geesthacht, Germany (53.5°N, 10.5°E)	May 1994–Mar 1996	34 cirrus cases
Sassen et al. (1990)	WI, United States (43°−45°N, 88°−91°W)	27–28 Oct 1986	Four lidar systems; 32 h with cirrus
Seifert et al. (2007)	Maldives, Indian Ocean (4.1°N, 73.3°E)	Feb 1999–Mar 2000	Four periods of intensive observation
Veerabuthiran and Satyanarayana (2004)	Trivandrum, India (8.6°N, 77°E)	Jun 1999–Apr 2003	190 days (~50% with cirrus)
Whiteman and Demoz (2004)	Andros Island, Bahamas (24.7°N, 77.8°W)	Jul–Sep 1998	220 h with cirrus
Winker and Vaughan (1994)	Hampton, VA (37.0°N, 76.5°W)	1989, 1991	1000 h (~50% with cirrus)
Wylie et al. (1995)	Madison, WI (43.1°N, 89.4°W)	Aug 1993–Apr 1994	19 cirrus cases

Cloud-Aerosol Lidar and IR Pathfinder Satellite Observations (CALIPSO; Winker et al. 2007), using 1 yr of statistics. This analysis has confirmed the results of Stubenrauch et al. (2005) showing that the peak of altitude difference distributions is around 0, but that the distribution for thin cirrus is broader than the one observed for thick cirrus.

For the comparisons with lidar results, we note that the statistics of TOVS Path-B contain both single-layered and multilayered clouds. The comparison with LITE has shown that at a spatial resolution of 1° in latitude and longitude, about two-thirds of the high-cloud occurrences involve multilayer cloud systems. In the case of multilayer clouds, the TOVS Path-B altitude of the highest cloud layer is retrieved; in general, this altitude is as well determined as in the case of single-layer thin cirrus.

3. Optical thickness of high clouds

a. Ground-based lidar observations

The seven datasets under consideration are compared in Fig. 3, in terms of cumulative frequency. Tropical sites are indicated by black symbols, and midlatitude sites are indicated by white and gray symbols for sites located in the continental United States and France, respectively. Additionally, Fig. 3 compares results obtained from both the MI and PI methods applied to observations conducted at Palaiseau.

TABLE 3. Selected high-cloud observations from surface-based lidar instrumentation.

	Gadanki[a]	Haute Provence[b]	Lannion[c]	Palaiseau[c,d]	Reunion[e]	Salt Lake City[f]	SGP CART[g]
Location	13.5°N, 79.2°E	43.9°N, 5.7°E	48.7°N, 3.5°W	48.7°N, 2.2°E	21.0°S, 55.5°E	40.8°N, 111.8°W	36.6°N, 97.5°W
Lidar and wavelength under consideration (nm)	Nd:YAG, 532	Nd:YAG, 532	Nd:YAG, 532	Nd:YAG, 532	Nd:YAG, 532	Ruby, 694	Raman, 355
Pulsed energy (mJ)	550	300	400	150	1000	1500	400
Field of view (detection; mrad)	1		1	0.5, 5	0.6	1	0.3, 3
Integration time (s)	250	160	2–32	30	120	120	600
Vertical resolution (m)	300	75	30	15	150	7.5	
Approach for integrating layer optical thicknesses; lidar ratio [LR (sr)]	PI method[h]; LR = 20	PI method; LR = 18.2	MI method[i]	MI and PI methods; LR temperature dependent	PI method; LR = 18.2	Sassen and Cho (1992)	Based on Ansmann et al. (1992)'s method
Multiple-scattering corrections	None	None	Chen et al. (2002)	Chen et al. (2002)	None	Cloud dependent	None
Period of observation	Mar 1998–Feb 2001	1997–99	Sep 2001–Jun 2005	Oct 2002–Feb 2006	1996–2001	1992–99	Nov 1996–Nov 2000
Duration of observation	195 nights	384 nights, ~2300 h	77 days	534 days	533 nights, 1643 h		
Strategy of observation	Nighttime only	Nighttime only; no deep low clouds	Near NOAA AVHRR overpasses; no low clouds	Basically daytime; all rainless weather	Nighttime only; no deep low clouds	After visual inspection by a trained observer	Continuous observation
Identification criteria of high clouds	Threshold on SR[j]	Threshold on SR and cloud temperature below −25°C	Base alt above 7 km	Base alt above 7 km	Threshold on SR and cloud temperature below −38°C	TAU above 0.05[k]	Base alt above 7 km and DELTA above 0.1[l]
Time span with high clouds	155 nights, ~416 h	206 nights	69 days	193 days, ~262 h	~115 h	~860 h	~1000 h

[a] See Sunilkumar et al. (2003).
[b] See Goldfarb et al. (2001).
[c] This study.
[d] See Noel and Haeffelin (2007).
[e] See Cadet et al. (2003).
[f] See Sassen and Comstock (2001).
[g] See Wang and Sassen (2002).
[h] PI (see section 2a).
[i] MI (see section 2a).
[j] SR is the scattering ratio, defined as the sum of the Mie (particles) and Rayleigh (molecules) backscattering coefficients, divided by the Rayleigh backscattering coefficient.
[k] Because of the limitations of the lidar and the IR radiometer method in assessing properties of optically thin clouds, Sassen and Comstock (2001) have rejected visible optical thicknesses below 0.05.
[l] DELTA is the lidar linear depolarization ratio, defined as the ratio of returned powers in the planes of the polarization orthogonal and parallel to that of the linearly polarized source.

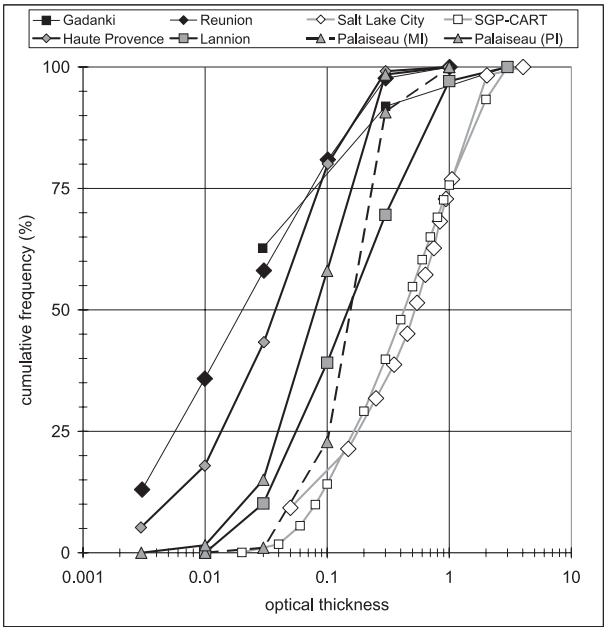

FIG. 3. Distribution of the optical thickness associated with high clouds, at the ground lidar sites summarized in Table 3. MI and PI indicate the results after applying these two methods to the same lidar observations at Palaiseau.

Cumulative frequencies for the tropical sites agree within 10%, with higher frequencies of cloud having optical thicknesses less than 0.1 than at midlatitude sites. Such a result (thin clouds are relatively more frequent at tropical than at other latitudes) is consistent with previous findings from spaceborne lidar observations (Eguchi et al. 2007). Results for midlatitude sites exhibit less agreement than for the tropical sites under consideration.

In reality, we should not expect similar cloud optical thickness distributions from lidar observations conducted under different regional atmospheric conditions. As discussed by Keckhut et al. (2006), a given high-cloud climatology is conditioned by the weather systems prevailing on the site under consideration because they determine to a large extent the variations in temperature, pressure, and water vapor content in air masses where clouds can subsequently form. For instance, Sassen and Campbell (2001) found that the strong linkage between cirrus and weather in Salt Lake City is controlled by upper-air circulations mainly related to seasonally persistent intermountain region ridge–trough systems.

Nevertheless, cloud optical thickness distributions from lidar observations are not exclusively dependent on regional atmospheric conditions. Particularly in the case of the datasets under consideration, there are several notable differences.

First, the observation strategy varied from the automatic recording (Palaiseau, SGP CART) to the human-dependent visual identification of ice clouds previous to lidar operation (Lannion, Salt Lake City). Subvisual clouds, with optical thicknesses smaller than 0.03 (Sassen and Cho 1992), may be undersampled according to the latter strategy.

Second, somewhat different cloud types are being compared. Five of seven datasets in Fig. 3 (Gadanki, Haute Provence, Réunion, Salt Lake City, and SGP CART) correspond explicitly to high clouds that contain ice particles only (''ice clouds''); nevertheless, the criteria adopted for identifying ice clouds were not unique. Such criteria were based on conditions to be fulfilled regarding the base altitude, the temperature at the base altitude, the scattering ratio, the linear depolarization, the visual appearance, or combinations of these parameters. The Lannion and Palaiseau datasets correspond to high clouds identified from the base altitude only, and then they may partially consist of liquid water particles.

Third, different methods were used to calculate cloud optical thickness, including (a) the molecular integration method, which involves the interpolation of the molecular backscatter profile above and below each cloud layer (Lannion and also Palaiseau), and (b) the particle integration method, which requires the specification of the lidar ratio associated with the cloud particles (Haute Provence, Palaiseau, Réunion). As shown by Cadet et al. (2005), the PI method is more reliable than the MI method for optical thicknesses smaller than 0.2.

Fourth, the instrumentation varied from one site to another. Each dataset corresponds to a particular combination of a suite of parameters like maximum pulsed energy, pulse width and its repetition rate, beam divergence, vertical resolution, noise level, integration time, and receiver solid angle. The role played by these parameters on cloud optical thickness remains to be assessed, and it is plausible that they can impact the observation of thin and thick clouds. For instance, while more powerful lidar systems have a higher sensitivity to cloud particles, there can be an increase in multiple scattering contributions to lidar return signals. The multiple scattering contributions increase with optical thickness and depend on the receiver solid angle (Platt 1981). However, little effort has been undertaken to include such an influence on the optical thickness evaluation [e.g., Sassen and Comstock (2001); Salt Lake City dataset]. A rough estimate of the forward-scattering influence is considered in the case of the Lannion and Palaiseau datasets (see section 2a).

Additionally, high-cloud optical thickness distributions from ground-based lidar observations can be different

because of methodological features, too. The evaluation of the latter influence is not straightforward, making comparisons involving two given sites difficult.

In the case of the Salt Lake City and SGP CART sites, distributions are close over a wide range of optical thicknesses despite differences in sampling atmospheric conditions (episodic and continuous recording), in identifying ice clouds (visual inspection and linear depolarization thresholds), and in accounting for multiple scattering effects (with and without, respectively). Disregarding for a moment these methodological features, both distributions indicate that the regional atmospheric conditions are less effective in producing optically thin high clouds (TAU < 0.1) than the conditions prevailing at the other sites under consideration.

In the case of Lannion and Palaiseau, optical thickness distributions disagree (by 10% or more) even after the application of the same approach for integrating backscatter profiles, the same (first order) multiple scattering corrections, and the same procedure for compiling daily events rather than individual atmospheric profiles. Consideration of instrumental issues and their compromises (resulting in different integration time values) and the observation strategy seem to be the major candidate ''methodological'' reasons for such disagreements. However, regional atmospheric features cannot be discarded. Because of the geographical location of these sites (Lannion is located a few kilometers from the sea), it may be argued that the prevailing atmospheric conditions are influenced by midlatitude storms traveling in the east Atlantic [see, e.g., typical trajectories shown in Fig. 5 of Joly et al. (1997)]. Application of such a hypothesis to the analysis of tenths of days with lidar observation under the occurrence of high clouds is far from straightforward.

Seasonal features are presented in Fig. 4 for selected midlatitude sites. Such a presentation, site by site (rather than season by season), allows a clearer analysis because the methodological factors affecting the cloud optical thickness distributions—instrumentation, observation strategy, integration method—remain unchanged. The Palaiseau and SGP CART datasets correspond to weaker seasonality, in the sense that similar cumulative frequencies were obtained. Recall that both datasets have an automated measurement strategy. In the case of Palaiseau, more than 100 days of lidar operation by season had been completed by February 2006 (see Table 1). We note that the Haute Provence and Lannion datasets exhibit different seasonal features. Both datasets have been built after the scientific-oriented selection of atmospheric conditions before starting the lidar operation. Table 1 shows that in the case of Lannion not only the seasonal distribution of the lidar operation has been very inhomogeneous (4.5 times more days in summer than in winter) but also such an operation has been very oriented toward high-cloud observations (90% of operation days corresponded to at least 10 observations with high clouds).

b. Spaceborne and ground-based lidar observations

For the sake of a proper comparison, we have limited our interest to GLAS observations for which the surface (land or sea) return was unambiguously identified. We kept only data for which the optical thickness of all the layers was available, and the altitude base of the lowest layer was above 7 km.

The upper-left panel in Fig. 5 compares the global distributions of high-cloud optical thickness, after separating the GLAS daytime (black) and nighttime backscatter profiles (gray line). Atmospheric background due to scattered sunlight can be strong enough to disturb observations performed with a spaceborne lidar, reducing its ability to detect optically thin clouds. As can be seen in Fig. 5, GLAS daytime observations do not show the occurrence of high clouds associated with optical thicknesses smaller than 0.02. The nighttime and daytime global distributions become closer after discarding optical thicknesses smaller than 0.02 in the nighttime distribution (crosses).

In the following discussion, only distributions of cloud optical thickness resulting from GLAS nighttime observations are considered. To obtain a sufficient number of GLAS observations, we focused on two latitude bands (20°S–20°N, and 40°–60°N), roughly corresponding to the locations of the ground sites.

In the upper-right panel in Fig. 5, three different criteria employed in identifying high clouds are compared for both latitude bands: base temperature colder than 233 K (black squares), base temperature colder than 253 K (white squares), and base altitude above 7 km (single-color curves). It is relevant to note that Eguchi et al. (2007) have identified cirrus clouds from GLAS observations through a criterion combining the base temperature and altitude. Eguchi et al. defined ice clouds after their base temperature (colder than 233 K), and adopted base-altitude thresholds of 5 and 8 km for midlatitudes and the tropics, respectively. As shown in our Fig. 5, base altitudes above 7 km and base temperatures colder than 253 K identify essentially the same clouds for both latitude bands. This is also the case after adopting a cloud-top temperature threshold of 233 K, as in Sassen et al. (2008) (results not shown). For both latitude bands, the importance of thin clouds (TAU < 0.01) increases in adopting 233 K instead 253 K as a base temperature threshold.

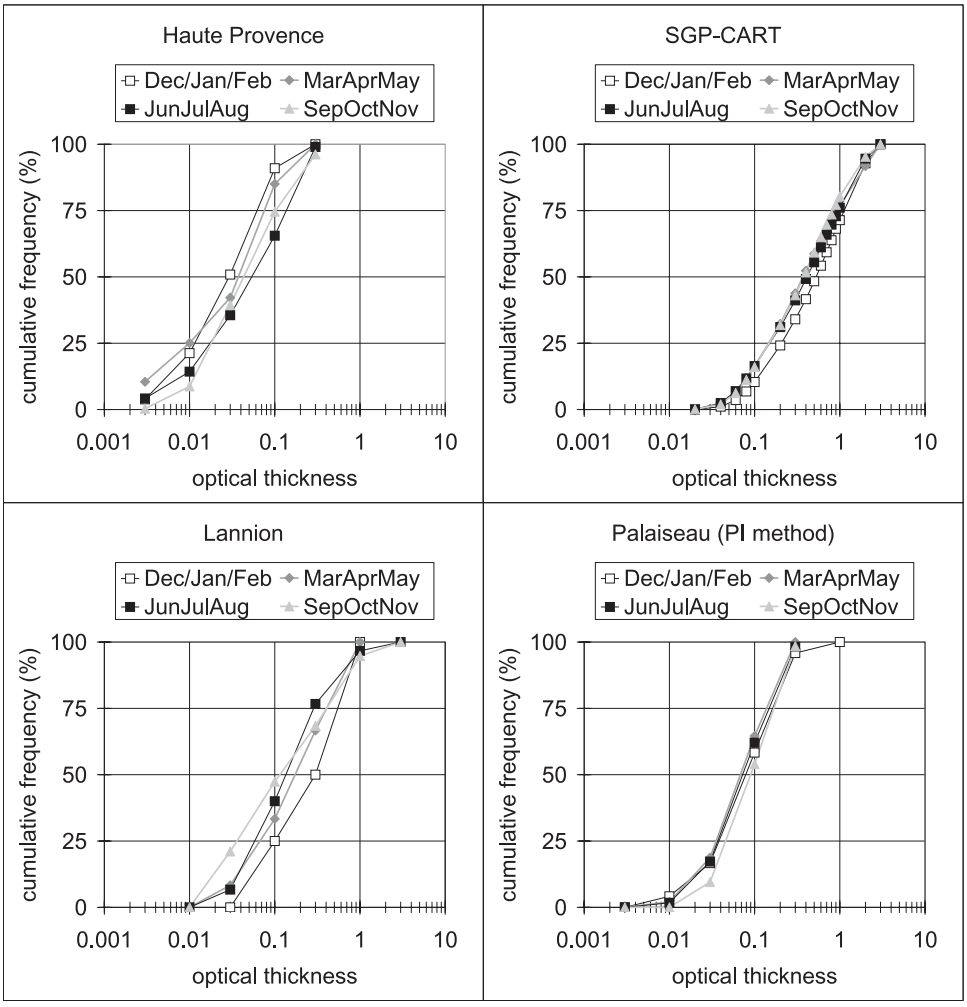

FIG. 4. Seasonal distribution of the optical thickness associated with high clouds, at four ground lidar sites under consideration.

In the following analysis, high clouds that were identified through their base altitude (lower threshold at 7 km) are considered from GLAS observations. In the center panel in Fig. 5, we have compared GLAS and ground lidar distributions of high-cloud optical thicknesses for the tropics and northern midlatitudes. For the latter, results from ground lidars come from different longitudes and prevailing cloud regimes (continental United States, France). Longitudinally integrated optical thicknesses from GLAS observations consistently correspond to cumulative frequencies that are intermediate to those from ground lidars. Differences between the optical thickness distributions are large for the tropics, where both ground lidar datasets characterize ice clouds (see Table 3). Such differences decrease as the base altitude of the GLAS selected high clouds increases from 7 to 12 km (see left-center panel in Fig. 5). Such an effect depends on the optical thickness itself, being greater at 0.1 than at 0.01. The small frequency of very thin (TAU $<$ 0.01) GLAS clouds compared to ground lidars might be associated with different cloud sensitivities. Nevertheless, a further analysis is limited by the regional limitation of ground lidar statistics as well as by the short time coverage of the GLAS dataset under consideration.

Section 3a compared high-cloud statistics at different sites from ground-based lidar observations. The latter have been performed with the help of different instrumentation, conducted according to different strategies, and analyzed through different methods. The operation of a spaceborne lidar system provides the possibility of investigating the respective statistics with the help of unique instrumentation, observation strategies, and methods of analysis. Moreover, spaceborne lidar observations likely provide a better assessment of cloud tops than those that are ground based.

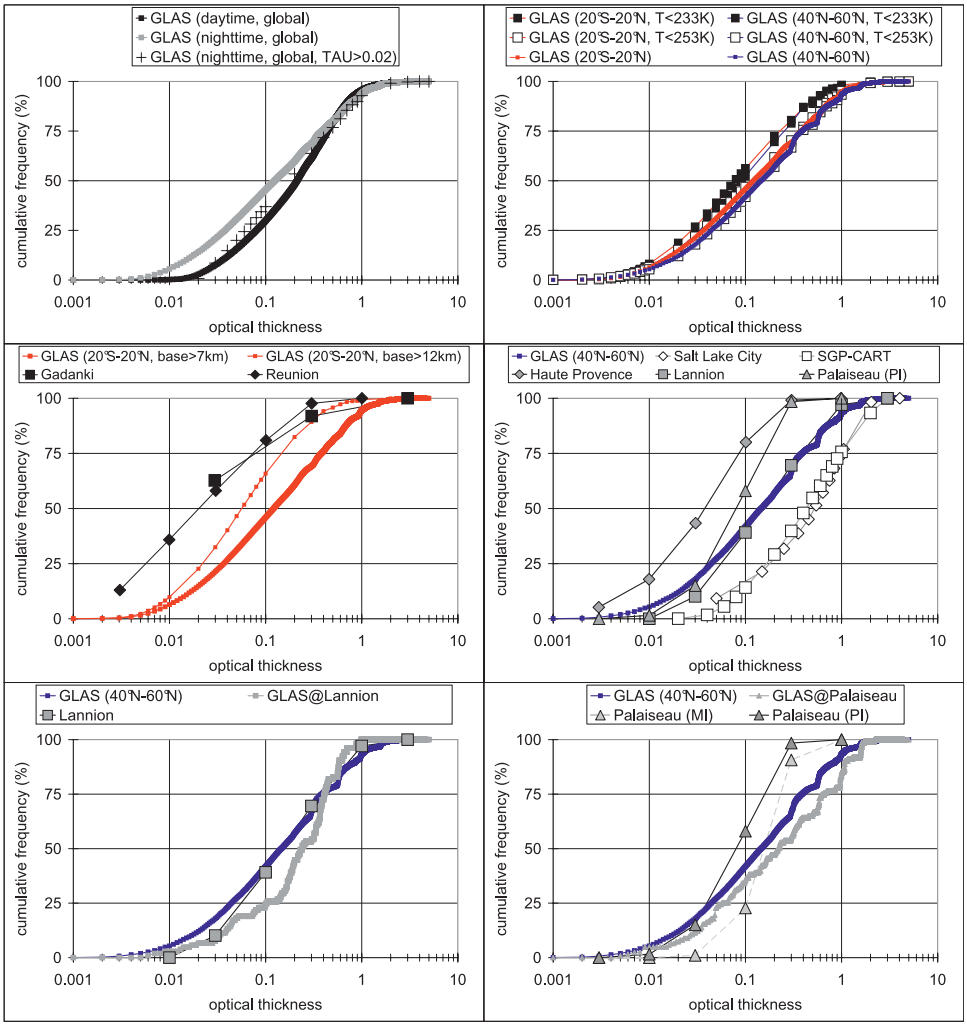

FIG. 5. Distributions of the optical thickness associated with high clouds from GLAS and selected ground lidar sites: (top left), global results (daytime, nighttime, and nighttime after discarding events corresponding to TAU < 0.02); (top right) latitude-averaged results after no temperature threshold, and after two temperature thresholds at cloud base; (middle) latitude-averaged distributions from GLAS and selected ground lidar sites at tropical and northern midlatitudes; and (bottom) a variety of GLAS and ground lidar results at (left) Lannion and (right) Palaiseau (see text).

Although more consistent, such an investigation has inherent limits, like some bias in sampling the diurnal cycle and sampling over a given time period. The bottom panels in Fig. 5 present a sensitivity test performed in an attempt to reduce the geographical domain under consideration for GLAS observations. As previously, blue lines in Fig. 5 indicate the longitudinally integrated optical thickness distribution from GLAS nighttime observations for the 40°–60°N latitude band. Regions extending over 3° in latitude and 6° in longitude centered on Lannion and Palaiseau were quite arbitrarily defined (not too large to be representative of the cloud cover properties over the site, not too small to have a sufficient number of GLAS observations). Thick gray lines show the resulting optical thickness distributions, obtained from 92 and 155 averaged profiles associated with high clouds, respectively, over Lannion and Palaiseau. Differences between respective GLAS optical thickness distributions reached 10% or more.

In summary, the optical thicknesses from GLAS and ground lidar are consistent on northern midlatitudes (center-right panel in Fig. 5); despite the variety of instruments, observation strategies, and methods of analysis employed by different research groups, no major bias can be attributed to such GLAS high-cloud statistics. Nevertheless, additional work remains to be accomplished in order to understand GLAS results in the tropics. Regional evaluation is a challenging task, requiring larger

and regular datasets as well as the adoption of homogeneous procedures and systems.

4. Altitude of high clouds

Cloud ''limits'' (e.g., bases and tops) depend on the radiation wavelength of the observation, because each particle size (and shape) interacts differently with the wavelengths used in atmospheric remote sensing. This is obvious for ice clouds observed simultaneously with the help of visible lidar and microwave radar (see, e.g., Fig. 4 in Haeffelin et al. 2005). Procedures for cloud altitude identification from lidar measurements have been developed and compared (e.g., Wang and Sassen 2001). Such an issue can be assumed to be negligible when comparing altitude statistics resulting from observations performed with two visible lidar systems, but becomes important when cloud-top estimates from visible lidar and infrared sounder spaceborne observations are compared (Stubenrauch et al. 2005).

Two comparison exercises are presented in this section, as contributions to a deeper understanding of high-cloud altitudes as estimated from different measuring systems. As a first exercise, selected lidar datasets are compared: ground-based observations at Lannion and Palaiseau, and latitude-integrated results from GLAS. Altitude estimates should agree better than their respective optical thickness estimates since they do not involve an integration method, a lidar ratio assumption, or a multiple scattering correction.

Figure 6 presents altitude and geometrical thickness distributions in a four-row, four-column display format. The first column (from the left) corresponds to the whole subdataset A of ground lidar high-cloud statistics (Table 1), while the three remaining columns show results for three ranges of cloud optical thickness (i.e., <0.03, between 0.03 and 0.3, and >0.3). These classes have been defined by Sassen and Cho (1992) in characterizing ice clouds. Variables displayed from the first to the fourth rows correspond to the highest top altitude, the mean altitude, the lowest base altitude, and the geometrical thickness distributions emerging from days corresponding to at least 10 ground lidar observations associated with high clouds. Results for Lannion (Palaiseau) are shown with green (blue) bars, excepting situations in which the number of days was considered to be arbitrarily small. Selected displays include respective information from the northern midlatitudes after analysis of nighttime GLAS observations (gray bars).

The ground lidar results agree for the intermediate range of optical thicknesses (0.03–0.3): daily values of the highest top, mean altitude, lowest base, and geometrical thickness peak near 11.5, 9.5, 7.5, and 1.5 km, respectively. The highest top and geometrical thickness assume slightly greater values, and the mean altitude and lowest base slightly lower values, at Lannion than at Palaiseau. It is difficult to separate the relative importance of the prevailing weather systems, of the observation strategy, and of the limited sample size on such small differences. Results associated with the whole range of optical thicknesses (left panels in Fig. 6) are somewhat dominated by those in the 0.03–0.3 range; the latter correspond to more than 59% and 83% of days under consideration, respectively, for Lannion and Palaiseau. In general, results obtained from Palaiseau indicate that optically thinner high clouds ($TAU < 0.03$) were associated with higher altitudes and smaller geometrical thicknesses. Results from Lannion show that optically thicker high clouds ($TAU > 0.3$) were also geometrically thicker (peaking near 2.5 rather than 1.5 km) and their tops were higher (peaking near 12.5 rather than 11.5 km).

Selected altitude and geometrical thickness distributions from GLAS observations were included in Fig. 6. Excepting mean altitudes corresponding to optically thin clouds, the agreement between the ground and space lidars is remarkable: their respective distributions peak within 1 km. More effort remains a requirement in comparing respective altitude estimates under other climatic conditions.

As a second exercise, thin cirrus altitude statistics from TOVS Path-B, covering a period of 8 yr, were compared to ground-lidar results at Lannion and Palaiseau. The former dataset corresponds to cloud altitudes above 8 km, and to visible optical thicknesses with TAU between 0.1 and 1.4 (see section 2d). Regions extending over 3° in latitude and 6° in longitude centered on Lannion and Palaiseau were taken into account. The optical thickness ranging from 0.1 to 1.4 and the lower base altitude threshold of 8 km were also adopted in the Lannion and Palaiseau ground-based datasets. As a result, among the 69 (193) days corresponding to at least 10 observations with high clouds associated with base altitude above 7 km and TAU between 0.003 and 3 at Lannion (Palaiseau), only 37 (79) days were retained, that is, about 54% (39%) of previously considered high clouds (see Table 1). Since TOVS Path-B retrievals are equally distributed over the year, a proper comparison with the results from ground-based lidars requires a sampling as uniform as possible throughout the year. The inspection of both ground lidar datasets revealed that such a condition was not fulfilled. The 37 (79) days with high clouds that were retained are distributed as 6, 6, 17, and 8 (10, 25, 19, and 25) for winter, spring, summer, and autumn, respectively, in the case of Lannion (Palaiseau).

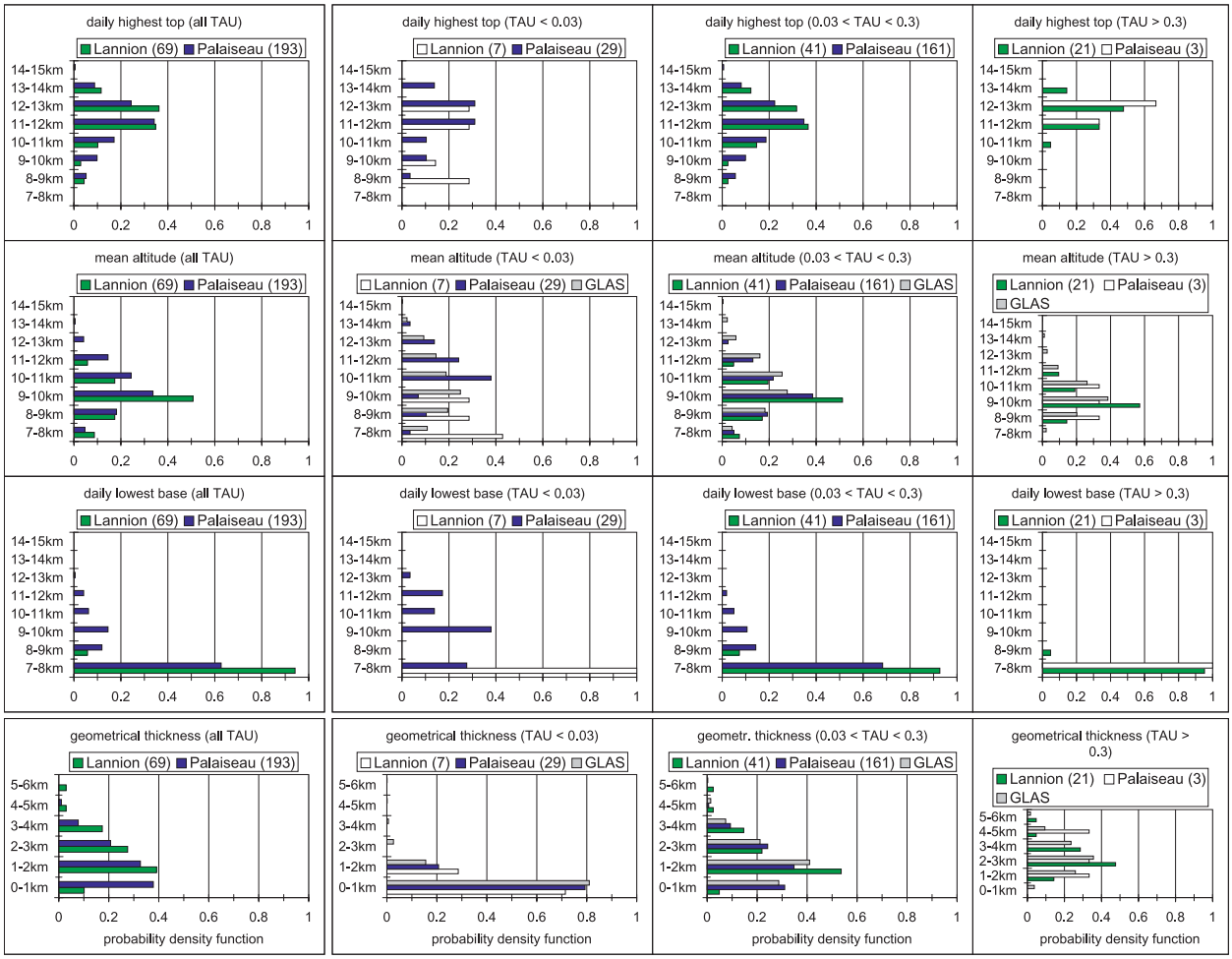

FIG. 6. Distributions of altitude and geometrical thickness associated with high clouds from ground lidars at Lannion (green) and Palaiseau (blue), and from GLAS nighttime observations for the latitude band 40°–60°N (gray bars). Figures in parentheses indicate the respective numbers of days corresponding to at least 10 observations associated with high clouds. Results displayed through white bars correspond to values of such numbers of days that were quite low (and hence their significance was smaller): (top to bottom) daily highest top, mean altitude, daily lowest base, and geometrical thickness; (left to right) all TAUs, TAU < 0.03, TAU < 0.3, and TAU > 0.3.

The top panels in Fig. 7 compare the distributions of thin cirrus altitude from the TOVS Path-B climatology (dashed bars) to those of the high-cloud mean altitude as obtained from ground lidar observations. The ordinates correspond to the vertical resolution of the TOVS Path-B altitude estimates. Ground lidar results are presented in Fig. 7 using three different statistics: the daily highest mean altitude (white), the daily median value of mean altitudes (gray), and the daily lowest mean altitude (black bars). Altitude estimates from TOVS Path-B agree better with the latter at both sites. The mean altitudes from ground lidar do not exceed 13.5 km at either site. In the TOVS Path-B retrieval, clouds for which the chi-2 method did not provide a physical solution have been set to very thin cirrus (or clear sky) with $E_{\mathrm{cld}} = 0$ and $P_{\mathrm{cld}} = 106$ hPa, the latter corresponding to the highest altitude value in Fig. 7. The three distributions from ground lidar highlight the diurnal variability of the altitude of cloud altitude. The bottom panels in Fig. 7 present geometrical thickness distributions of high clouds associated with the daily minimum and daily maximum mean altitude. Over Lannion, both distributions are quite similar and broad. Over Palaiseau, the geometrical thickness of the lowest clouds is slightly smaller than that for the highest clouds.

Whereas the high-cloud altitude distributions with no cloud layers underneath are relatively symmetric with peak values at 9.5–11.5 km from both ground lidar datasets (daily median values of mean altitudes, top panels in Fig. 7), the altitude distributions for thin cirrus from TOVS Path-B are strongly asymmetric, with peak

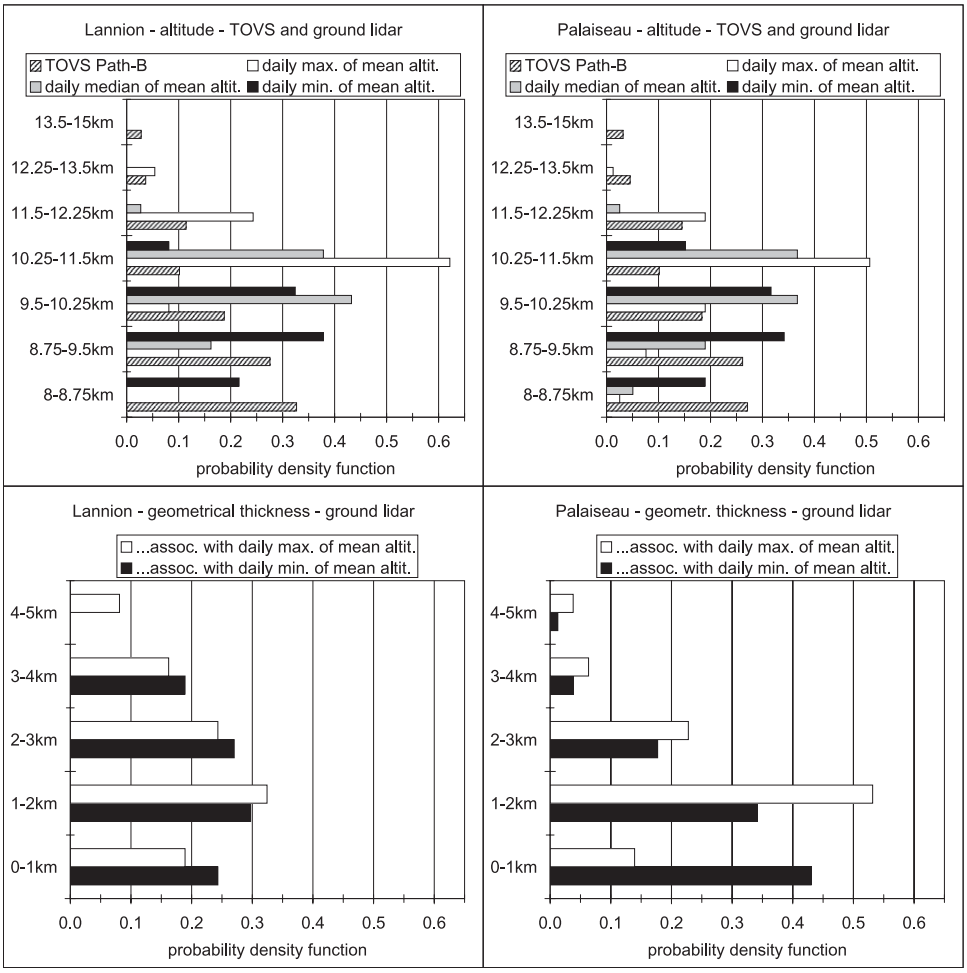

FIG. 7. Distributions of the altitude and of the geometrical thickness associated with high clouds at (left) Lannion and (right) Palaiseau. Analysis is restricted to days corresponding to at least 10 observations with high clouds, associated with base altitude above 8 km and an optical thickness between 0.1 and 1.4 (see text). (top) Comparison of altitude estimates from TOVS Path-B and daily maximum, median, and minimum values of the mean high-cloud altitude from ground-based lidar observations. (bottom) The geometrical thicknesses that correspond to the daily minimum and maximum of the mean altitudes.

values at 8–9.5 km. There are three reasons that could explain the discrepancies:

1) The atmospheric conditions under consideration are different: thin cirrus with no cloud layer underneath from ground-based lidar observations are compared with thin cirrus from TOVS Path-B. The latter corresponds in a large fraction (more than two-thirds) to multilayer cloud systems. An independent analysis (N. Lamquin, Laboratoire de Météorologie Dynamique, 2008, personal communication) of 1 yr of CALIPSO L2 data (Winker et al. 2007) sampled over the Palaiseau site shows a nearly symmetric distribution peaked at 10 km. In the case of multilayer high clouds (half of the cases with layers separated by more than 800 m), the altitude distribution of the highest cloud is slightly shifted to lower altitude values.
2) The statistics of the datasets are very different: the TOVS Path-B climatology provides measurements twice per day over 8 yr, whereas the ground-based lidar observations were only performed on selected days, in total 37 and 79 days, respectively, for Lannion and Palaiseau.
3) The uncertainty of the TOVS Path-B altitude determination for thin cirrus is larger than for thick cirrus.

A further comparison is presented in Fig. 8, for the latitude band 40°–60°N. The thin cirrus altitude from TOVS Path-B is compared to the middle altitude of the highest cloud layer with optical thicknesses between 0.1 and 1.4 as seen from LITE and GLAS observations,

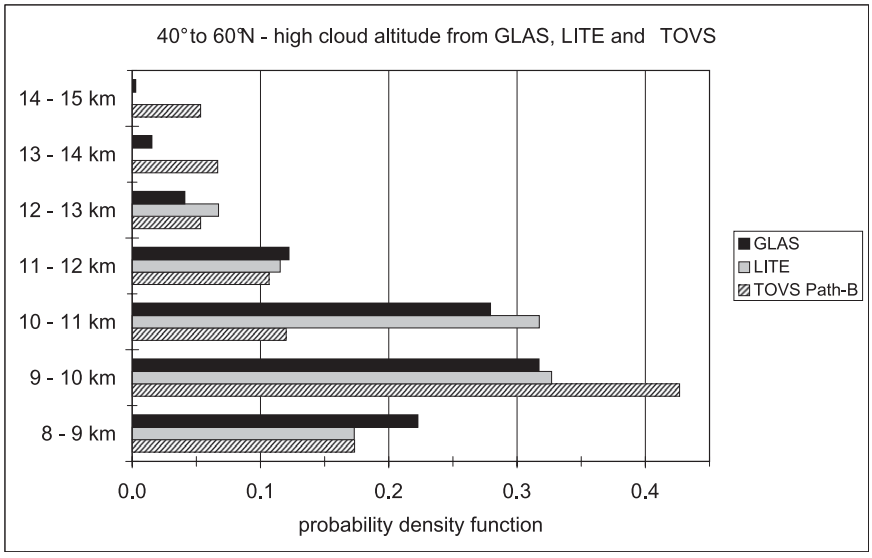

FIG. 8. Distributions of the middle altitude of the highest cloud layer from GLAS (black bars) and from LITE observations (gray bars), and of the cloud altitude estimated from TOVS Path-B (dashed); all distributions are averaged over 40°–60°N.

with no exclusion of cases with cloud layers underneath. TOVS Path-B and LITE distributions correspond both to the 10 days of LITE operation in September 1994 (see further details in Stubenrauch et al. 2005), whereas the GLAS data correspond to October–November 2003. The distributions agree quite well, with a peak around 9.5 km.

5. Summary and recommendations

The statistical description (''climatology'') of clouds occurring in the upper troposphere (''high clouds'') has been the goal of a number of earlier studies. A variety of measuring systems have been employed in evaluating their optical thickness and altitude. Crucial points in these comparisons are (i) the effects of varying instrument sensitivity and measurement strategies on the retrieval of optically thin cirrus, (ii) the statistical meaningfulness of the dataset, and (iii) the restriction of measurements in the case of multiple layer cloud systems.

Our main findings can be summarized as follows:

1) Cloud optical thickness distributions from two tropical ground lidar sites (Gadanki in India, and Réunion Island in the Indian Ocean) agree, with both indicating more thin high clouds than at midlatitudes. Results from five midlatitude sites (Haute Provence, Lannion, Palaiseau, Salt Lake City, and SGP CART) exhibit a relatively large variation. Regional atmospheric conditions certainly play a role in explaining such a variation, although notable differences exist among the datasets under consideration regarding lidar observation strategy and data processing.
2) The top, mean, and base altitudes, as well as the geometrical thickness of high clouds, were studied as a function of the optical thickness using ground lidar observations at Lannion and Palaiseau. No major disagreement was noted between these sites.
3) Optical thickness distributions from a spaceborne lidar system (GLAS) and ground lidar sites are consistent at northern midlatitudes despite the variety of instruments, observation strategies, and methods of analysis employed in establishing five high-cloud statistics from ground-based measurements. The reduced sample size inherent in the GLAS observations in boreal autumn 2003 did hindered a deeper comparison, site to site, with ground-based optical thickness distributions.
4) Altitudes of thin cirrus from the 8-yr cloud TOVS Path-B climatology, resulting from the processing of spaceborne infrared sounder observations, were compared with mean altitudes of high clouds (a) with no lower clouds underneath, (b) with cloud altitudes higher than 8 km, and (c) with $0.1 < \mathrm{TAU} < 1.4$, from ground-based lidar measurements at Lannion and Palaiseau. From all days corresponding to at least 10 observations with high clouds observed at Lannion (Palaiseau), 54% (39%) correspond to this category, which roughly agrees with 40% of thin cirrus out of all high clouds observed by TOVS in

these regions. The distribution of the altitude of thin cirrus obtained from the TOVS Path-B climatology is asymmetric, with a peak between 8 and 9.5 km, whereas the ground-based lidar climatologies provide symmetric distributions with a peak between 9.5 and 11.5 km. Spaceborne lidar measurements provide distributions with peaks around 10 km. Single-layer high clouds from ground-based lidar observations seem to be slightly higher and thinner relative to the total (spaceborne) statistics. This is a result that needs to be investigated further using collocated datasets.

Moreover, some recommendations for future work emerged during the development of this study.

1) High-cloud statistics from ground-based lidar measurements could be more effectively compared after the adoption of a common observation strategy. If continuous recording cannot be implemented, efforts should be undertaken toward improving the seasonal sampling. Because of the difficulty in standardizing human visual inspection, it would be preferable to record continuously even for a few hours so as to not automatically discard the thinnest subvisual clouds. A number of routine ground-based lidar observation programs are being conducted, among them the Micro Pulse lidar Network (MPLNet; Campbell et al. 2002), whose results shall be included in a future study.
2) High-cloud optical thickness distributions from lidar measurements could be more effectively compared after the application of a common method for integrating layer optical thicknesses, or at least methods following a similar approach. If taken into account, multiple scattering corrections and temperature influences on lidar ratio could be presented in more detail, allowing proper comparisons with sensitivity tests on selected parameters.

The synergy between ground-based and spaceborne lidar observations should be explored in future studies by including instruments like CALIOP aboard CALIPSO (Winker et al. 2007). As noted by Sassen et al. (2008), thin cloud layers that have been ignored by ground-based instruments (because of attenuation due to the presence of an optically thick lower cloud layer) could be more properly observed from a spaceborne lidar. Observations using infrared sounders are complementary on the optical thickness scale, and this fact could constitute the starting point of more robust climatologies of high clouds in the near future. This is also the case for back-scattered and limb-viewing transmitted solar radiation observations, as well as for observations performed through lidars and radars. The combination of results from two, three, or more of these measuring systems appears to be a sensible approach toward fully characterizing the entire family of high clouds on the global scale.

Acknowledgments. The first author thanks the Laboratoire d'Optique Atmosphérique, where this work was initiated. The authors acknowledge Z. Wang and K. Sassen for making available their data for Salt Lake City and SGP-CART sites; M. Lalande for help with the GLAS data; G. Swiathy for help with the data for the Lannion site; and A. Protat and Y. Lemaître for helpful discussions. This research was partially supported by Délégation Générale pour l'Armement, MIRA Grant 03.34.035.00.470.75.65, with additional support from the ONERA (the French Aerospace Laboratory). We thank the National Snow and Ice Data Center (NSIDC), the ICARE Data and Services Center, and CLIMSERV for providing access to the GLAS data used in this study. Final acknowledgments are addressed to the anonymous reviewers and to the editor (B. Baum), whose constructive criticism significantly improved our manuscript.

REFERENCES

Abshire, J. B., X. Sun, H. Riris, J. M. Sirota, J. F. McGarry, S. Palm, D. Yi, and P. Liiva, 2005: Geoscience Laser Altimeter System (GLAS) on the ICESat mission: On-orbit measurement performance. *Geophys. Res. Lett.,* **32,** L21S02, doi:10.1029/2005GL024028.

Ansmann, A., U. Wandinger, M. Riebesell, C. Weitkamp, and W. Michaelis, 1992: Independent measurement of extinction and backscatter profiles in cirrus clouds by using a combined Raman elastic-backscatter lidar. *Appl. Opt.,* **31,** 7113–7131.

——, and Coauthors, 1993: Lidar network observations of cirrus morphological and scattering properties during the International Cirrus Experiment 1989: The 18 October 1989 case study and statistical analysis. *J. Appl. Meteor.,* **32,** 1608–1622.

Beyerle, G., H.-J. Schafer, R. Neuber, O. Schrems, and I. S. McDermid, 1998: Dual wavelength lidar observation of tropical high-altitude cirrus clouds during the ALBATROSS 96 campaign. *Geophys. Res. Lett.,* **25,** 919–922.

——, and Coauthors, 2001: A lidar and backscatter sonde measurement campaign at Table Mountain during February–March 1997: Observations of cirrus clouds. *J. Atmos. Sci.,* **58,** 1275–1287.

Cadet, B., L. Goldfarb, D. Faduilhe, S. Baldy, V. Giraud, P. Keckhut, and A. Réchou, 2003: A sub-tropical cirrus cloud climatology from Réunion Island (21°S, 55°E) lidar data set. *Geophys. Res. Lett.,* **30,** 1130, doi:10.1029/2002GL016342.

——, V. Giraud, M. Haeffelin, P. Keckhut, A. Rechou, and S. Badly, 2005: Improved retrievals of the optical properties of cirrus clouds by a combination of lidar methods. *Appl. Opt.,* **44,** 1726–1734.

Campbell, J. R., D. L. Hlavka, E. J. Welton, C. J. Flynn, D. D. Turner, J. D. Spinhirne, V. S. Scott III, and I. H. Hwang, 2002: Full-time, eye-safe cloud and aerosol lidar observation at

Atmospheric Radiation Measurement Program sites: Instruments and data processing. *J. Atmos. Oceanic Technol.,* **19,** 431–442.

Chahine, M. T., and Coauthors, 2006: AIRS: Improving weather forecasting and providing new data on greenhouse gases. *Bull. Amer. Meteor. Soc.,* **87,** 912–926.

Chazette, P., J. Pelon, and G. Mégie, 2001: Determination by spaceborne backscatter lidar of the structural parameters of atmospheric scattering layers. *Appl. Opt.,* **40,** 3428–3440.

Chen, W.-N., C.-W. Chiang, and J.-B. Nee, 2002: Lidar ratio and depolarization ratio for cirrus clouds. *Appl. Opt.,* **41,** 6470–6476.

Chervet, P., and A. Roblin, 2006: High-altitude cloud effects on airborne electro-optical sensor performance. *J. Atmos. Oceanic Technol.,* **23,** 1530–1538.

Comstock, J. M., T. P. Ackerman, and G. G. Mace, 2002: Ground-based lidar and radar remote sensing of tropical cirrus clouds at Nauru Island: Cloud statistics and radiative impacts. *J. Geophys. Res.,* **107,** 4714, doi:10.1029/JD002203.

DelGuasta, M., M. Morandi, L. Stefanutti, J. Brechet, and J. Piquad, 1993: One year of cloud lidar data from Dumont d'Urville (Antarctica). 1. General overview of geometrical and optical properties. *J. Geophys. Res.,* **98,** 18 575–18 587.

Dessler, A. E., and P. Yang, 2003: The distribution of tropical thin cirrus clouds inferred from *Terra* MODIS data. *J. Climate,* **16,** 1241–1247.

Eguchi, N., T. Yokota, and G. Inoue, 2007: Characteristics of cirrus clouds from ICESat/GLAS observations. *Geophys. Res. Lett.,* **34,** L09810, doi:10.1029/2007GL029529.

Flamant, P., G. Brogniez, M. Desbois, Y. Fouquart, J.-F. Flobert, J.-C. Vanhoutte, and U. Nat Singh, 1989: High altitude cloud observations by ground-based lidar, infrared radiometer and METEOSAT measurements. *Ann. Geophys.,* **7,** 1–10.

Giannakaki, E., V. Amiridis, and D. Balis, 2004: Cirrus measurements with a Raman lidar over Thessaloniki, Greece, during EARLINET. *Proc. 22th Int. Laser Radar Conf.,* Matera, Italy, ESA SP 561, 37–40.

Gobbi, G. P., F. Barnaba, and L. Ammannato, 2004: The vertical distribution of aerosols, Saharan dust and cirrus clouds in Rome (Italy) in the year 2001. *Atmos. Chem. Phys.,* **4,** 351–359.

Goldfarb, L., P. Keckhut, M.-L. Chanin, and A. Hauchecorne, 2001: Cirrus climatological results from lidar measurements at OHP (44°N, 6°E). *Geophys. Res. Lett.,* **28,** 1687–1690.

Haeffelin, M., and Coauthors, 2005: SIRTA, a ground-based atmospheric observatory for cloud and aerosol research. *Ann. Geophys.,* **23,** 253–275.

Hlavka, D. L., S. P. Palm, W. D. Hart, J. D. Spinhirne, M. J. McGill, and E. J. Welton, 2005: Aerosol and cloud optical depth from GLAS: Results and verification for an October 2003 California fire smoke case. *Geophys. Res. Lett.,* **32,** L22S07, doi:10.1029/2005GL023413.

Imasu, R., and Y. Iwasaka, 1991: Characteristics of cirrus clouds observed by laser radar (lidar) during the spring of 1987 and the winter of 1987/88. *J. Meteor. Soc. Japan,* **69,** 401–410.

Immler, F., and O. Schrems, 2002a: Determination of tropical cirrus properties by simultaneous LIDAR and radiosonde measurements. *Geophys. Res. Lett.,* **29,** 2090, doi:10.1029/2002GL015076.

——, and ——, 2002b: LIDAR measurements of cirrus clouds in the northern and southern midlatitudes during INCA (55°N, 53°S): A comparative study. *Geophys. Res. Lett.,* **29,** 1809, doi:10.1029/2002GL015077.

Joly, A., and Coauthors, 1997: The Fronts and Atlantic Strom-Track Experiment (FASTEX): Scientific objectives and experimental design. *Bull. Amer. Meter. Soc.,* **78,** 1917–1940.

Keckhut, P., F. Borchi, S. Bekki, A. Hauchecorne, and M. SiLaouina, 2006: Cirrus classification at midlatitude from systematic lidar observations. *J. Appl. Meteor. Climatol.,* **45,** 249–258.

McCormick, M. P., and Coauthors, 1993: Scientific investigations planned for the Lidar In-Space Technology Experiment (LITE). *Bull. Amer. Meteor. Soc.,* **74,** 205–214.

McFarquhar, G. M., A. J. Heymsfield, J. Spinhirne, and B. Hart, 2000: Thin and subvisual tropopause tropical cirrus: Observations and radiative impacts. *J. Atmos. Sci.,* **57,** 1841–1853.

Morille, Y., M. Haeffelin, P. Drobinski, and J. Pelon, 2007: STRAT: An automated algorithm to retrieve the vertical structure of the atmosphere from single-channel lidar data. *J. Atmos. Oceanic Technol.,* **24,** 761–775.

Noel, V., and M. Haeffelin, 2007: Midlatitude cirrus clouds and multiple tropopauses from a 2002–2006 climatology over the SIRTA observatory. *J. Geophys. Res.,* **112,** D13206, doi:10.1029/2006JD007753.

——, D. M. Winker, T. J. Garrett, and M. McGill, 2007: Extinction coefficients retrieved in deep tropical ice clouds from lidar observations using a CALIPSO-like algorithm compared to in-situ measurements from the cloud integrating nephelometer during CRYSTAL-FACE. *Atmos. Chem. Phys.,* **7,** 1415–1422.

Pace, G., M. Cacciani, A. di Sarra, G. Fiocco, and D. Fua, 2003: Lidar observations of equatorial cirrus clouds at Mahe Seychelles. *J. Geophys. Res.,* **108,** 4236, doi:10.1029/2002JD002710.

Palm, S., W. Hart, D. Hlavka, E. J. Welton, and J. Spinhirne, 2002: Geoscience Laser Altimeter System (GLAS) atmospheric data products—Algorithm theoretical basis document (version 4.2). Goddard Space Flight Center, Greenbelt, MD, 137 pp.

Parameswaran, K., S. V. Sunilkumar, B. V. Krishna Murthy, and K. Satheesan, 2004: Lidar observations of high altitude cirrus clouds near the tropical tropopause. *Adv. Space Res.,* **34,** 845–850.

Platt, C. M. R., 1973: Lidar and radiometric observations of cirrus clouds. *J. Atmos. Sci.,* **30,** 1191–1204.

——, 1981: Remote sensing of high clouds. III: Monte Carlo calculations of multiple-scattered lidar returns. *J. Atmos. Sci.,* **38,** 156–167.

——, and A. C. Dilley, 1979: Remote sounding of high clouds: II. Emissivity of cirrostratus. *J. Appl. Meteor.,* **18,** 1144–1150.

——, S. C. Scott, and A. C. Dilley, 1987: Remote sounding of high clouds. Part VI: Optical properties of midlatitude and tropical cirrus. *J. Atmos. Sci.,* **44,** 729–747.

——, and Coauthors, 1994: The Experimental Cloud Lidar Pilot Study (ECLIPS) for cloud-radiation research. *Bull. Amer. Meteor. Soc.,* **75,** 1635–1654.

——, S. A. Young, P. J. Manson, G. R. Patterson, S. C. Marsden, R. T. Austin, and J. H. Churnside, 1998: The optical properties of equatorial cirrus from observations in the ARM Pilot Radiation Observation Experiment. *J. Atmos. Sci.,* **55,** 1977–1996.

——, ——, R. T. Austin, G. R. Patterson, D. L. Mitchell, and S. D. Miller, 2002: LIRAD observations of tropical cirrus clouds in MCTEX. Part I: Optical properties and detection of small particles in cold cirrus. *J. Atmos. Sci.,* **59,** 3145–3162.

Reichardt, J., 1999: Optical and geometrical properties of northern midlatitude cirrus clouds observed with a UV Raman lidar. *Phys. Chem. Earth,* **24B,** 255–260.

Rossow, W. B., and R. A. Schiffer, 1999: Advances in understanding clouds from ISCCP. *Bull. Amer. Meteor. Soc.,* **80,** 2261–2287.

Sassen, K., and B. S. Cho, 1992: Subvisual-thin cirrus lidar dataset for satellite verification and climatological research. *J. Appl. Meteor.,* **31,** 1275–1285.

——, and S. Benson, 2001: A midlatitude cirrus cloud climatology from the Facility for Atmospheric Remote Sensing. Part II: Microphysical properties derived from lidar depolarization. *J. Atmos. Sci.,* **58,** 2103–2112.

——, and J. R. Campbell, 2001: A midlatitude cirrus cloud climatology from the Facility for Atmospheric Remote Sensing. Part I: Macrophysical and synoptic properties. *J. Atmos. Sci.,* **58,** 481–496.

——, and J. M. Comstock, 2001: A midlatitude cirrus cloud climatology from the Facility for Atmospheric Remote Sensing. Part III: Radiative properties. *J. Atmos. Sci.,* **58,** 2113–2127.

——, C. J. Grund, J. D. Spinhirne, M. M. Hardesty, and J. M. Alvarez, 1990: The 27–28 October 1986 FIRE IFO cirrus case study: A five lidar overview of cloud structure and evolution. *Mon. Wea. Rev.,* **118,** 2288–2311.

——, J. M. Comstock, Z. Wang, and G. G. Mace, 2001: Cloud and aerosol research capabilities at FARS: The Facility for Atmospheric Remote Sensing. *Bull. Amer. Meteor. Soc.,* **82,** 1119–1138.

——, J. Zhu, and S. Benson, 2003: Midlatitude cirrus cloud climatology from the Facility for Atmospheric Remote Sensing. IV. Optical displays. *Appl. Opt.,* **42,** 332–341.

——, L. Wang, D. O'C. Starr, J. M. Comstock, and M. Quante, 2007: A midlatitude cirrus cloud climatology from the Facility for Atmospheric Remote Sensing. Part V: Cloud structural properties. *J. Atmos. Sci.,* **64,** 2483–2501.

——, Z. Wang, and D. Liu, 2008: Global distribution of cirrus clouds from CloudSat/Cloud-Aerosol Lidar and Infrared Pathfinder Satellite Observations (CALIPSO) measurements. *J. Geophys. Res.,* **113,** D00A12, doi:10.1029/2008JD009972.

Schutz, B. E., H. J. Zwally, C. A. Shuman, D. Hancock, and J. P. DiMarzio, 2005: Overview of the ICESat mission. *Geophys. Res. Lett.,* **32,** L21S01, doi:10.1029/2005GL024009.

Scott, N. A., and Coauthors, 1999: Characteristics of the TOVS Pathfinder Path-B dataset. *Bull. Amer. Meteor. Soc.,* **80,** 2679–2701.

Seifert, P., A. Ansmann, D. Muller, U. Wandinger, D. Althausen, A. J. Heymsfield, S. T. Massie, and C. Schmitt, 2007: Cirrus optical properties observed with lidar, radiosonde, and satellite over the tropical Indian Ocean during the aerosol-polluted northeast and clean maritime southwest monsoon. *J. Geophys. Res.,* **112,** D17205, doi:10.1029/2006JD008352.

Spinhirne, J. D., S. P. Palm, W. D. Hart, D. L. Hlavka, and E. J. Welton, 2005a: Cloud and aerosol measurements from GLAS: Overview and initial results. *Geophys. Res. Lett.,* **32,** L22S03, doi:10.1029/2005GL023507.

Stubenrauch, C. J., A. Chédin, R. Armante, and N. A. Scott, 1999a: Clouds as seen by infrared sounders (3I) and imagers (ISCCP). Part II: A new approach for cloud parameter determination in the 3I algorithms. *J. Climate,* **12,** 2214–2223.

——, W. B. Rossow, N. A. Scott, and A. Chedin, 1999b: Clouds as seen by satellite sounders (3I) and imagers (ISCCP). Part III: Spatial heterogeneity and radiative effects. *J. Climate,* **12,** 3419–3442.

——, F. Eddounia, and L. Sauvage, 2005: Cloud heights from TOVS Path-B: Evaluation using LITE observations and distributions of highest cloud layers. *J. Geophys. Res.,* **110,** D19203, doi:10.1029/2004JD005447.

——, A. Chedin, G. Radel, N. A. Scott, and S. Serrar, 2006: Cloud properties and their seasonal and diurnal variability from TOVS Path-B. *J. Climate,* **19,** 5531–5553.

——, S. Cros, N. Lamquin, R. Armante, A. Chédin, C. Crevoisier, and N. A. Scott, 2008: Cloud properties from Atmospheric Infrared Sounder and evaluation with Cloud-Aerosol Lidar and Infrared Pathfinder Satellite Observations. *J. Geophys. Res.,* **113,** D00A10, doi:10.1029/2008JD009928.

Sunilkumar, S. V., K. Parameswaran, and B. V. Krishna Murthy, 2003: Lidar observations of cirrus cloud near the tropical tropopause: General features. *Atmos. Res.,* **66,** 203–227.

Veerabuthiran, S., and M. Satyanarayana, 2004: Lidar observations of cirrus clouds at low latitude tropical station, Trivandrum (8°33′N, 77°E): General characteristics. *Proc 22th Int. Laser Radar Conf.,* Matera, Italy, ESA SP 561, 399–402.

Wang, Z., and K. Sassen, 2001: Cloud type and macrophysical property retrieval using multiple remote sensors. *J. Appl. Meteor.,* **40,** 1665–1682.

——, and ——, 2002: Cirrus cloud microphysical property retrieval using lidar and radar measurements. Part II: Midlatitude cirrus microphysical and radiative properties. *J. Atmos. Sci.,* **59,** 2291–2302.

Whiteman, D. N., and B. Demoz, 2004: Subtropical cirrus cloud extinction to backscatter ratios measured by Raman lidar during CAMEX-3. *Geophys. Res. Lett.,* **31,** L12105, doi:10.1029/2004GL020003.

Winker, D. M., and M. A. Vaughan, 1994: Vertical distribution of clouds over Hampton, Virginia observed by lidar under the ECLIPS and FIRE ETO programs. *Atmos. Res.,* **34,** 117–133.

——, and C. R. Trepte, 1998: Laminar cirrus observed near the tropical tropopause by LITE. *Geophys. Res. Lett.,* **25,** 3351–3354.

——, W. H. Hunt, and M. J. McGill, 2007: Initial performance assessment of CALIOP. *Geophys. Res. Lett.,* **34,** L19803, doi:10.1029/2007GL030135.

Wylie, D. P., and W. P. Menzel, 1999: Eight years of cloud statistics using HIRS. *J. Climate,* **12,** 170–184.

——, ——, H. M. Woolf, and K. I. Strabala, 1994: Four years of global cirrus cloud statistics using HIRS. *J. Climate,* **7,** 1972–1986.

——, P. Piironen, W. Wolf, and E. Eloranta, 1995: Understanding satellite cirrus cloud climatologies with calibrated lidar optical depths. *J. Atmos. Sci.,* **52,** 4327–4343.

Young, S. A., 1995: Analysis of lidar backscatter profiles in optically thin clouds. *Appl. Opt.,* **34,** 7019–7031.